Materials Science in Semiconductor Processing 27 (2014) 1036–1041

Contents lists available at ScienceDirect

Materials Science in Semiconductor Processing

journal homepage: www.elsevier.com/locate/mssp

Fast photocatalytic degradation of an organic dye and photoluminescent properties of Zn doped $In(OH)_3$ obtained by the microwave-assisted hydrothermal method

M.T.S. Tavares [a,*], L.X. Lovisa [a], V.D. Araújo [a], E. Longo [b], M.S. Li [c], R.M. Nascimento [a], C.A. Paskocimas [a], M.R.D. Bomio [a], F.V. Motta [a]

[a] LSQM—Laboratório de síntese química de materiais - DEMAT, UFRN, Campus Lagoa Nova, CEP 59078-900 Natal, RN, Brazil
[b] LIEC—Laboratório interdisciplinar de eletroquímica e cerâmica, UFSCar, São Carlos Rua Francisco Degni s/n, CEP 14801-907 Araraquara, SP, Brazil
[c] IFSC—Instituto de Física de São Carlos, USP, São Paulo, Av. Trabalhador São-carlense, Centro, CEP 13566-590, São Carlos, SP, Brazil

ARTICLE INFO

Available online 27 September 2014

Keywords:
Indium hydroxide
Zinc
Doping
Microwave
Photocatalytic activity

ABSTRACT

Crystalline zinc-doped indium hydroxide structures were prepared by the rapid and efficient microwave-assisted hydrothermal (MAH) method. X-ray diffraction (XRD), field emission gun-scanning electron microscopy (FEG-SEM), photoluminescence (PL) and UV–visible (UV–vis) spectroscopy were used to characterization the materials. FEG-SEM images revealed that pure $In(OH)_3$ samples and Zn-doped samples exhibit nanocubic morphologies with a wide range of particle sizes. Relative intensities of PL emissions decreased as the Zn ion concentration increased from 0 to 4 mol%. UV–vis spectra indicate that Zn ion doping caused a band gap decrease with increased doping of 0% to 4% Zn, respectively, from 5.15 eV for 4.96 eV. Samples with Zn in the crystal lattice showed better photocatalytic activity and degradation of the RhB dye after 16 min of UV exposure.

1. Introduction

Nanostructured $In(OH)_3$ with uniform particle size and shape has generated intensive investigations due to its contribution to the understanding of novel physical properties and potential applications in several fields such as optoelectronics, information storage, catalysis, sensors and solar cells [1–7]. The indium hydroxide semiconductor has a wide gap (E_g) estimated to be 5.15 eV [8,9], especially in its nanostructure form, and has created intensive interest in its semiconducting and optical properties [10].

Doping semiconductors with different elements are known to greatly affect many of their basic physical properties (e.g., their electrical, optical and magnetic properties) which are crucial in most practical applications [11]. The efficiency of the dopant element depends on its electronegativity and ionic radius; also, it is strongly influenced by the synthesis method [12]. To obtain desired properties, in recent years, many researchers focused on the synthesis of doped and pure nanocrystalline semiconductors such as $In(OH)_3$ [13], ZnO [14–20], TiO_2 [21–23] and In_2O_3 [24].

Recently, $In(OH)_3$ nanoparticles were prepared by several synthesis methods such as the sol–gel technique [25], the hydrolysis of indium nitrate [26], thermal decomposition [27], spray pyrolysis [28] and the hydrothermal method [10,29,30].

The microwave-assisted hydrothermal (MAH) method has unique advantages such as uniform, fast and volumetric

* Corresponding author. Tel.: +55 84 3342 2512; fax: +55 84 3342 2406.
E-mail address: maratatianest@gmail.com (M.T.S. Tavares).

http://dx.doi.org/10.1016/j.mssp.2014.08.034
1369-8001/

heating as compared to other methods and has been efficiently used for the preparation of inorganic materials [31]. Furthermore, this method can significantly reduce the reaction time and the use of high temperatures which promotes rapid crystallization and simplifies the process of preparing nanoparticles [32–36]. Recently, the microwave-assisted hydrothermal method was successfully employed to obtain $In(OH)_3$ [13,37–39]. Motta et al. [13] synthesized $In(OH)_3$ Tb-doped structures with concentrations of $x=0$, 1, 2, 4 and 8 mol% of Tb^{3+} using the microwave-assisted hydrothermal method at a low temperature of 140 °C for 30 min.

Pál et al. [40] obtained a ZnO–$In(OH)_3$ nanocomposite by using the conventional hydrothermal treatment for 3 h; results showed that the PL nanocomposite doped with 1% $In(OH)_3$ showed better properties as compared to the pure ZnO matrix. Two additional blue emission bands with a maximum at 421 nm and 440 nm were also observed.

In summary, this study reports the synthesis of In $(OH)_3$:xZn structures doped with $x=0$, 1, 2 and 4 mol% of Zn using the microwave-assisted hydrothermal method at a low temperature of 140 °C for 30 min. In addition, to enlarge our understanding of their fundamental properties, the photoluminescence and photocatalytic properties of Zn doped $In(OH)_3$ nanostructures were investigated.

2. Experimental

2.1. Materials

Indium nitrate ($In(NO_3)_3 \cdot H_2O$, Alfa Aesar 99%), zinc nitrate ($Zn(NO_3)_2 \cdot H_2O$ Fluka, 99%), potassium hydroxide (KOH, Fluka, 99%) and distilled water were used as received to prepare zinc-doped indium hydroxide nanoparticles.

2.2. Preparation of $In(OH)_3$ nanoparticles

The experimental procedure is as follows: 7 mmol of indium nitrate and zinc nitrate was dissolved in 80 mL of deionized water under constant stirring for 20 min. The ion Zn was added in the following percentages: 0, 1, 2 and 4 mol%. The pH of the solution was adjusted to 11 by adding potassium hydroxide (6 M). The mixture was transferred into a Teflon autoclave which was sealed, and the reaction system was heated under hydrothermal temperature conditions at 140 °C for 30 min (the heating rate was fixed at 25 °C/min) using microwave irradiation (2.45 GHz and a maximum power of 800 W). The pressure in the autoclave was stabilized at 3.0 atm. The white product obtained by the MAH treatment was centrifuged, washed with distilled water and ethanol and finally dried at room temperature.

2.3. Characterization of $In(OH)_3$ nanoparticles

The powders were characterized by XRD using a Shimadzu diffractometer (Model XRD-7000, CuKα radiation ($\lambda=1.54$ Å), 40 kV and 30 mA and 2θ from 5° to 80°. The $In(OH)_3$ morphology and size were observed by FEG-SEM (Carl Zeiss, Supra 35-VP Model, Germany) images. UV–vis reflectance spectra of $In(OH)_3$ powders were taken using Cary 5G equipment. PL spectra were measured using a Thermal Jarrel-Ash Monospec 27 monochromator and Hamamatsu R446 photomultiplier. The 350.7 nm line of a krypton ion laser (Coherent Innova 90K) was used as the excitation source with the output power of the lasers kept at 200 mW. All measurements were taken at room temperature.

2.4. Photocatalytic activity

Photocatalytic properties of $In(OH)_3$ crystals (as a catalyst agent) for the degradation of Rhodamine B (RhB) dye with a molecular formula [$C_{28}H_{31}ClN_2O_3$] (99.5% purity, Mallinckrodt) in an aqueous solution were tested under UV-light illumination. About 50 mg of catalyst crystals was placed in a 250 mL beaker, and 50 mL of RhB solution (1×10^{-5} mol L^{-1}) pH 4 was added. These suspensions were ultrasonicated for 10 min in an ultrasonic cleaner before illumination and then stored in dark for 5 min to allow the saturated absorption of RhB onto the catalyst. The beakers were placed in a photo-reactor at controlled temperature (20 °C), under magnetic stirring, and were illuminated by six UVC lamps (TUV Philips, 15 W, with maximum intensity at 254 nm). The power light was measured by Coherent Power Max Model No PM10, and the optical energy density value was 20 mW cm^{-2}. At 2 min intervals, one 3 mL aliquot of these suspensions was removed and centrifuged at 9000 rpm for 5 min to remove particles in suspension. Finally, variations of the maximum absorption band of supernatant solutions were monitored by UV–vis absorbance spectra measurements using a double-beam spectrophotometer with double monochromator and a JASCO photomultiplier tube detector (model V-660, USA).

3. Results and discussion

XRD patterns of $In(OH)_3$ nanostructures with different percentages of Zn prepared by the MAH method at 140 °C for 30 min are shown in Fig. 1. XRD was used to verify the composition and phase evolution of the samples. All

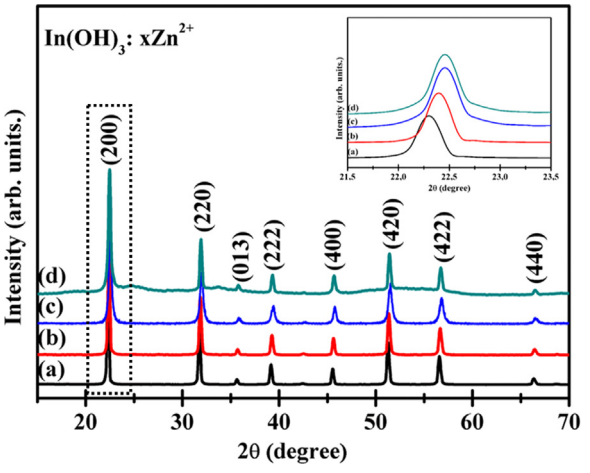

Fig. 1. XRD patterns of $In(OH)_3$:xZn powders obtained by the MAH method at 140 °C for 30 min: (a) $x=0$, (b) $x=1$, (c) $x=2$ and (d) $x=4$ mol%. Inset: shift around the (220) peak.

diffraction peaks in XRD patterns could be indexed to the cubic lattice related to the $In(OH)_3$ phase (PDF card no. 16-161). Secondary phases were not found in our samples despite the zinc doping up to 4 mol%, which is a first indicative that Zn ions were incorporated into $In(OH)_3$ nanocrystals.

Sample's crystallite sizes were estimated from the Scherrer equation [41] and full-width half-maximum (FWHM) of an observed peak. The strongest peak (200) was used to calculate the average crystallite size (D) of In $(OH)_3$ particles. Table 1 describes the lattice parameter a, unit cell volume V and crystallite size D for $In(OH)_3$:xZn samples. An increase in the crystallite size with increasing zinc content is observed. The lattice parameter (a) and the unit cell volume (V) decreased slightly with increasing zinc content, which can be related to the substitution of bigger In^{3+} ion (radii = 0.80 Å) by the smaller Zn^{2+} ion (radii = 0.74 Å) [42].

The size and morphology of the as-synthesized products were characterized by FEG-SEM (see Fig. 2). FEG-SEM image in Fig. 2a indicates that pure $In(OH)_3$ is composed mainly of microcubes with irregularly-shaped structures. When Zn ion was introduced into the $In(OH)_3$ array, no significant change in the morphology of $In(OH)_3$ was observed (Fig. 2b–d). In the literature, researchers [10,43,44] reported the syntheses of $In(OH)_3$ particles with cube-shaped morphology obtained with different particle sizes by thermal and/or convention hydrothermal treatments. In this study, the same cube-shaped morphology was synthesized in a short reaction time (30 min) which demonstrates the high capability of MAH in the achievement of cube-shaped $In(OH)_3$:xZn particles.

Table 1
Lattice parameters and the structural analysis results for the $In(OH)_3$:xZn samples.

$In(OH)_3$:xZn (mol%)	a (Å)	$2\theta_{(200)}$	$FWHM_{(200)}$	V (Å^3)	D (nm)
x:0	7.9683 ± 0.0004	22.304	0.1378	505.93 ± 0.07	2.95
x:1	7.9539 ± 0.0004	22.414	0.1378	503.21 ± 0.07	2.95
x:2	7.9463 ± 0.0004	22.475	0.1282	502.21 ± 0.07	3.17
x:4	7.9439 ± 0.0004	22.480	0.1181	501.31 ± 0.07	3.43

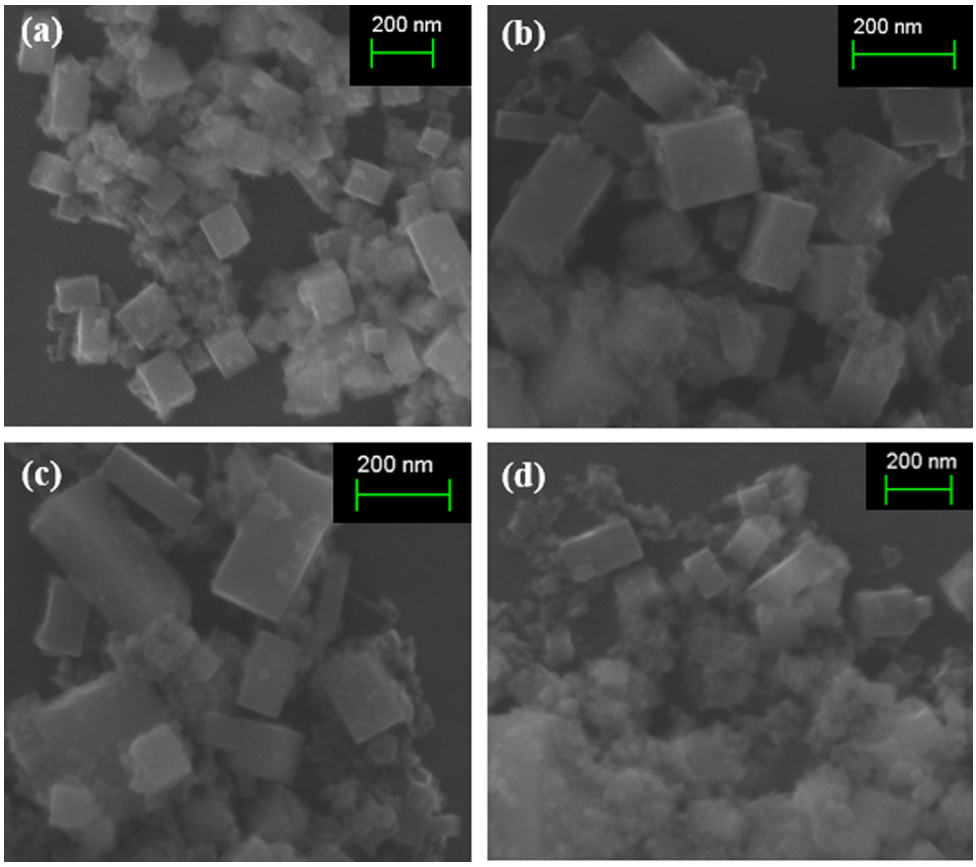

Fig. 2. FE-SEM images of $In(OH)_3$:xZn powders: (a) x = 0, (b) x = 1, (c) x = 2, and (d) x = 4 mol%.

$In(OH)_3$:*x*Zn samples were also examined by UV–visible diffuse reflectance. The optical band gap estimation was obtained by using the Wood and Tauc equation [45]. Estimated optical band gap values as a function of Zn concentration were 5.13, 5.08, 5.14 and 4.96 eV for pure In $(OH)_3$ and with 1, 2 and 4 mol% Zn, respectively. A comparison of the pure $In(OH)_3$ (5.13 eV) and $In(OH)_3$:4% Zn (4.96 eV) illustrates that the increase in the percentage of ion Zn causes a reduction in E_{gap} (see insets in Fig. 4b and c). Defects and impurities introduce energy levels into the band gap that allow transitions of lower energy and also lead to a decrease in E_{gap} [46]. Particularly in our samples, an increase in the content of oxygen vacancies to preserve electron neutrality is expected due to the substitution of In^{3+} ions by the lower valence Zn^{2+}, thus increasing the amount of defects in the sample which may lead to the decrease in the band gap.

Fig. 4 shows PL spectra of $In(OH)_3$:*x*Zn samples obtained at room temperature with an excitation wavelength of 350 nm. The PL is mainly attributed to oxygen vacancies or interstitial oxygen defects [47]. The broad and intense band covering a large part of visible spectra (from 400 to 650 nm) is visible for all samples which can be attributed to blue–green colors with the maximum intensity located at 453 nm. Yan et al. [29] showed a broad PL blue–green emission at 480 nm for $In(OH)_3$ nanocubes synthesized by the hydrothermal method at 120 °C for 12 h. According to literature reports [48,49], the blue luminescence emission mechanism of ZnO:$In(OH)_3$ is mainly attributed to the existence of oxygen vacancies in $In(OH)_3$ V_O° or $In(OH)_3$ $V_O^{\circ\circ}$. These oxygen vacancies normally act as deep defect donors in semiconductors and would induce the formation of new energy levels in the band gap. Both $In(OH)_3$ and $In(OH)_3$:Zn samples, obtained by the MAH method, were crystalline at long-range order which is in agreement with XRD analyses. However, maximum PL emission differences between obtained samples show that these differences occur in materials synthesized by the MAH method, which creates additional levels above the valence band (VB) and below the conduction band (CB). Then we can identify two effects in the PL emission of the samples. The first effect is intrinsic to $In(OH)_3$ material and is derived from the $In(OH)_3$ V_O^x that is constituted by asymmetric distorted complex cluster vacancies. The second effect is a consequence of doping $In(OH)_3$ by Zn which results in negatively charged clusters that eliminate oxygen vacancies. This fact shows that the doped sample has a different density of defects and just a different ability to generate pairs (e'–$h^{\bullet}$). This behavior can be related to reduction in the energy band gap values ($In(OH)_3$ to 5.13 eV and $In(OH)_3$:Zn to 4.96 eV) as well as the decrease in the intensity of the main band after doping, indicating that In ions can be substituted by Zn ions. On the other hand, created electron–hole pairs are more stable and could decrease the PL intensity in doped sample. The blue emission thus results from the radioactive recombination of photo-excited holes and electrons occupying the oxygen vacancies. The profile of the emission band is typical of a multiphonon and multilevel process where a system relaxation occurs by several paths involving the participation of numerous states

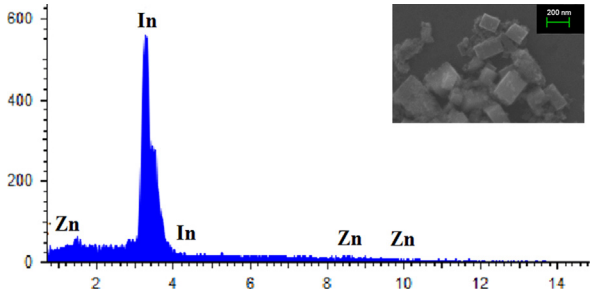

Fig. 3. EDS the sample $In(OH)_3$ with 4% Zn obtained at 140 °C for 30 min.

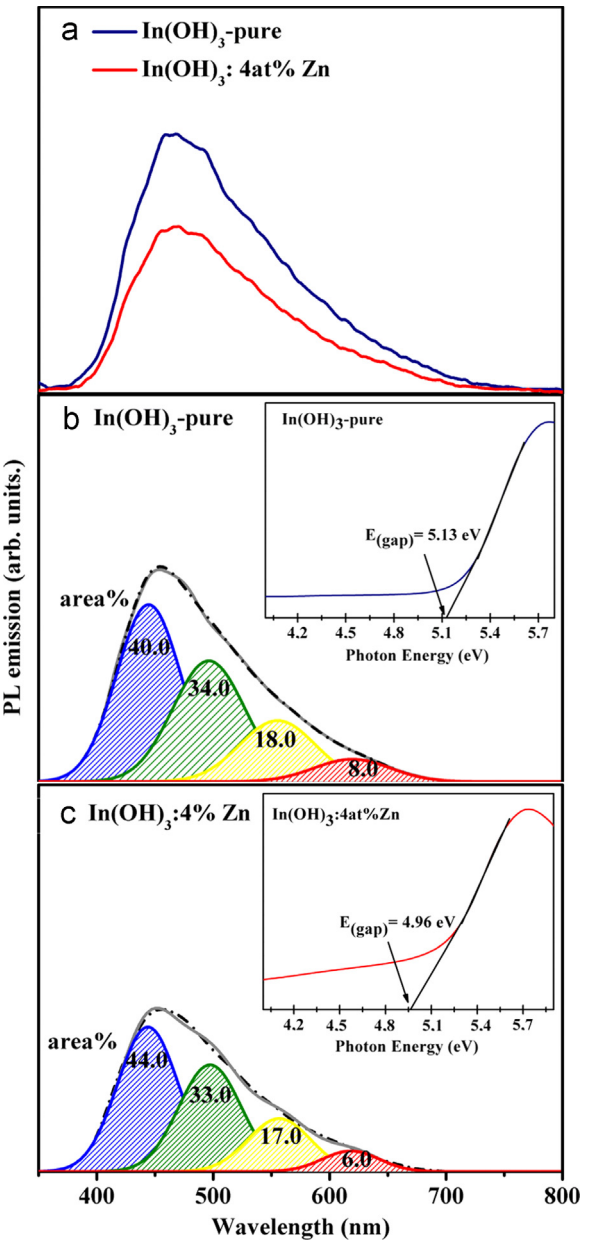

Fig. 4. (a) PL spectra of pure $In(OH)_3$ and $In(OH)_3$ with 4% Zn obtained at 140 °C for 30 min, (b)–(c) PL deconvolution curves of pure $In(OH)_3$ and In $(OH)_3$ samples with 4% Zn, respectively. (UV–vis reflectance spectra are shown in the inset (b)–(c)).

within the band gap of the material [50]. Using the Gaussian method, PL curves of the pure and doped $In(OH)_3$ sample were decomposed into five components which refer to the region in the visible spectrum where its maximum peak intensity appears (see Fig. 3b–c). PL curves shown in Fig. 4 were composed of four bands; a blue band (~440 nm), a green band (~500 nm), a yellow band (~556 nm) and an orange band (~625 nm) which specifies the region where the maxima of the component appears. Each color represents different types of electronic transition and is linked to a specific structural arrangement. PL emission results from the recombination of free charge carriers; generally, a weaker PL intensity implies a lower electron–hole recombination rate and corresponds to higher photocatalytic activity [51].

$In(OH)_3$ has recently been studied as a photocatalyst [52,53]. The doped $In(OH)_3$ was shown to be a visible-light-driven photocatalyst for hydrogen production from water [54]. Recent results showed that $In(OH)_3$ alone and doped $In(OH)_3$ both have likewise excellent photocatalytic activities for the photodegradation of organic pollution under UV and visible light irradiation, respectively [55,56]. The photoactivity of $In(OH)_3$ and 4% Zn doped samples was evaluated by the photocatalytic degradation of RhB under UV irradiation. Fig. 5 shows the degradation of the dye over time under UV radiation, and also photographs of the dye with and without catalysts (see inset in Fig. 5). The rate constant values are reported in Table 2.

For pure $In(OH)_3$, the RhB dye was totally photodegraded after only 30 min under UV light illumination, displaying a rate constant of 1.0×10^{-1} min^{-1}. This result indicates that even without any doping, the RhB photodegradation efficiency is high. On the other hand, for the sample 4% Zn doped sample, the photodegradation rate of RhB dye was higher than the pure $In(OH)_3$, proven by higher rate constant (2.9×10^{-1} min^{-1}), due to the action of defects in the crystal lattice caused by doping, which promoted remarkable changes in the degradation of the RhB dye. To further understand how defects improve photocatalytic properties, when light with a higher or equal energy to the band gap is irradiated to the semiconductor surface, a photo-excited VB electron is promoted to the CB and leaves behind a hole in the VB to create electron–hole pairs which are efficiently separated by the large electric field before recombination and causes a lower PL intensity (see Fig. 4) as well as an increase in the photocatalytic activity. Then, defects benefit the efficient separation of the generation of the (e^-/h^+) pairs, which promotes the formation of hydroxyl radicals (radical OH*) and superoxide radical anions (O_2H^*). These radicals are oxidizing species in photocatalytic oxidation processes. During the photocatalytic process, the hydroxyl radical is recognized as the most powerful oxidizing species [57–59] which can attack organic pollutants near the photocatalyst surface and can transform them into water and carbon dioxide. A high charge separation rate is beneficial for the formation of the hydroxyl radical which favors the decolorization of RhB. Detailed results of adsorption spectra during the photocatalytic degradation process of pure In $(OH)_3$ and doped Zn are displayed in Fig. 6. Mechanisms of formation of possible radicals are as follows:

$$O_2 + e^- \rightarrow O_2^{\bullet -} \quad (1)$$

$$O_2^{\bullet -} + H^+ \rightarrow HO_2\bullet \quad (2)$$

$$HO_2\bullet + HO_2\bullet \rightarrow H_2O_2 + O_2 \quad (3)$$

$$H_2O_2 + e_{cb}^- \rightarrow HO^\bullet \rightarrow HO^\bullet + HO^- \quad (4)$$

$$H_2O_2 + O_2\bullet \rightarrow HO^\bullet + HO^- + O_2 \quad (5)$$

$$H_2O_2 \rightarrow 2HO^\bullet \quad (6)$$

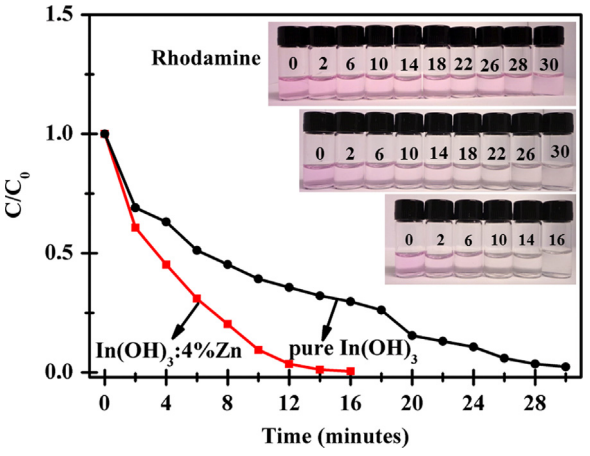

Fig. 5. Effects of different times on degradation of the rhodamine dye of pure $In(OH)_3$ and $In(OH)_3$ with 4% Zn (photographs of the evolution of dye degradation are shown in the inset) (1 g/L catalyst initial concentration and 1×10^{-5} mol/L dye initial concentration, pH 4).

Table 2
Rate constants, *k*, for $In(OH)_3$ and $In(OH)_3$:4% Zn samples.

Sample	Rate constants *k* (min^{-1})
Rhodamine (no catalyst)	1.9×10^{-2}
$In(OH)_3$	1.0×10^{-1}
$In(OH)_3$:4% Zn	2.9×10^{-1}

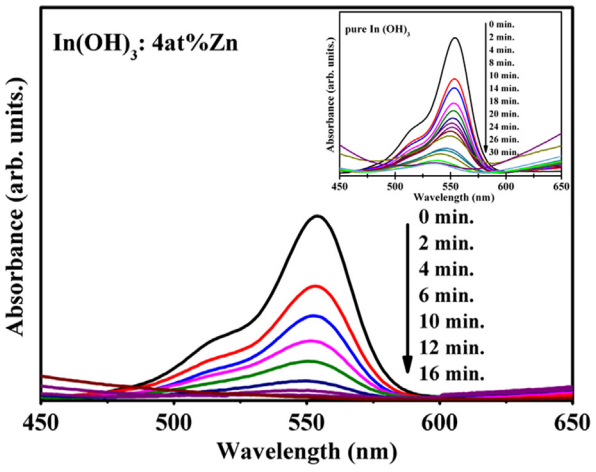

Fig. 6. Photocatalytic degradation the rhodamine dye of pure $In(OH)_3$ and $In(OH)_3$ with 4% Zn (1 g/L catalyst initial concentration and 1×10^{-5} mol/L dye initial concentration, pH 4).

$$O_2 + HO^- \rightarrow O_{2^\bullet} + HO^\bullet \quad (7)$$

$$Dye + OH \rightarrow Degradation\ products \quad (8)$$

$$Dye + h_{VB} \rightarrow Oxidation\ products \quad (9)$$

$$Dye + e_{CB} \rightarrow Reduction\ products \quad (10)$$

4. Conclusions

In(OH)$_3$:*x*Zn powders (where $x=0$, 1, 2 and 4 mol%) were efficiently obtained in their crystalline phase using the MAH method at 140 °C for 30 min. As shown in FEG-SEM images, this preparation strategy for In(OH)$_3$ nanocubes has proven to be a simple and effective synthesis method. Pure In(OH)$_3$ sample has the highest PL intensity while the 4% Zn/In(OH)$_3$ sample has the lowest PL intensity. These PL results are consistent with the photocatalytic activity of the products. These optical properties exhibited by In(OH)$_3$:*x*Zn suggest that this material is a highly promising candidate for photoluminescent and photocatalytic applications.

Acknowledgments

The authors gratefully acknowledge the financial support of the Brazilian governmental research funding agencies CAPES, Brazil and CNPq. Brazil (Grant no. 141890/2013-4).

References

[1] P. Jiang, J.F. Bertone, V.L. Colvin, Science 291 (2001) 453–457.
[2] Y. Huang, X. Duan, Y. Cui, et al., Science 294 (2001) 1313–1317.
[3] D.F. Wang, Z.G. Zou, J.H. Ye, Chem. Mater. 17 (2005) 3255–3261.
[4] K.R. Reyes-Gil, E.A. Reyes-Garcia., D. Raftery, J. Phys. Chem. C 111 (2007) 14579–14588.
[5] N. Pinna, G. Neri, M. Antonietti, et al., Angew. Chem. Int. Ed. 43 (2004) 4345–4349.
[6] G. Neri, A. Bonavita, G. Micali, et al., Chem. Commun. 48 (2005) 6032–6034.
[7] R. Katoh, A. Furube, T. Yoshihara, et al., J. Phys. Chem. B 108 (2004) 4818–4822.
[8] S. Avivi, Y. Mastai, A. Gedanken, Chem. Mater. 12 (2000) 1229–1233.
[9] T. Ishida, K. Kuwabara, J. Ceram. Soc. Jpn. 106 (1989) 381–384.
[10] H. Zhu, Y. Wang, N. Wang, et al., Mater. Lett. 58 (2004) 2631–2634.
[11] R. Yousefi, F. Jamali-Sheini, A.K. Zak, et al., Ceram. Int. 39 (2013) 5191.
[12] S. Cimitan, S. Albonetti, L. Forni, et al., J. Colloid Interface Sci. 329 (2009) 73–80.
[13] F.V. Motta, A.P.A. Marques, M.S. Li, et al., J. Alloys Compd. 553 (2013) 338–342.
[14] S.Y. Bae, C.W. Na, J.H. Kang, et al., J. Phys. Chem. B 109 (2005) 2526–2531.
[15] C.H. Jung, D.J. Kim, Y.K. Kang, et al., Thin Solid Films 517 (2009) 4078–4081.
[16] E. Pál, V. Hornok, A. Oszkoó, et al., Colloids Surf. A: Physicochem. Eng. Asp. 340 (2009) 1–9.
[17] M.N. Jung, S.H. Ha, S.J. Oh, et al., Curr. Appl. Phys. 9 (2009) e169–e172.
[18] R. Yousefi, F. Jamali-Sheini, A.K. Zak, et al., Ceram. Int. 38 (2012) 6295–6301.
[19] C. Xu, J. Chun, D. Kim, et al., Appl. Phys. Lett. 91 (2007) 153104.
[20] K.C. Barick, M. Aslam, V.P. Dravi, et al., J. Colloid Interface Sci. 349 (2010) 19–26.
[21] R. Asahi, T. Morikawa, T. Ohwaki, et al., Science 293 (2001) 269–271.
[22] H. Irie, Y. Wanatabe, K. Hashimoto, J. Phys. Chem. B 107 (2003) 5483–5486.
[23] J.C. Yu, J. Yu, W. Ho, et al., Chem. Mater. 14 (2002) 3808–3816.
[24] D.P. Dutta, V. Sudarsan, P. Srinivasu, et al., J. Phys. Chem. C 112 (2008) 6781–6785.
[25] A. Gurloa, M. Ivanovskayaa, N. Bârsan, et al., Sens. Actuators B: Chem. 44 (1997) 327–333.
[26] X.H. Zhang, S.Y. Xie, Z.M. Ni, et al., Inorg. Chem. Commun. 6 (2003) 1445–1447.
[27] H. Zhou, W. Cai, L. Zhang, Mater. Res. Bull. 34 (1999) 845–849.
[28] J.J. Prince, S. Ramamurthy, B. Subramanian, et al., J. Cryst. Growth 240 (2002) 142–151.
[29] T. Yan, X. Wang, J. Long, et al., J. Colloid Interface Sci. 325 (2008) 425–431.
[30] B. Li, Y. Xie, M. Jing, et al., Langmuir 22 (2006) 9380–9385.
[31] X. Hu, G. Li, J.C. Yu, Langmuir 26 (2010) 3031–3039.
[32] P.C. Ma, S.Y. Mo, B.Z. Tang, et al., Carbon 48 (2010) 1824–1834.
[33] L. Li, X. Zhang, W. Zhang, et al., Colloids Surf. A: Physicochem. Eng. Asp. 457 (2014) 134–141.
[34] L. Li, L. Wang, T. Hu, et al., J. Solid State Chem. 218 (2014) 81–89.
[35] F.V. Motta, A.P.A. Marques, V.D. Araújo, et al., Mat. Res. (Epub 13-Jun-2014). ISSN 1516–1439 (2014).
[36] E.B. Hostetler, K.J. Kim, R.P. Oleksak, et al., Mater. Lett. 128 (2014) 54–59.
[37] N. Koga, T. Kimizu, J. Am. Ceram. Soc. 91 (2008) 4052.
[38] F.V. Motta, R.C. Lima, A.P.A. Marques, et al., Mater. Res. Bull. 45 (2010) 1703.
[39] F.V. Motta, R.C. Lima, A.P.A. Marques, et al., J. Alloys Compd. 497 (2010) L25.
[40] E. Pál, V. Hornok, R. Kun, et al., J. Colloid Interface Sci. 378 (2012) 100–109.
[41] L.V. Azároff, Elements of X-ray crystallographyMcGraw-Hill Book Company, New York, EUA, 1968.
[42] R. Shannon, Acta Crystallogr. Sect. A 32 (1976) 751–767.
[43] S.E. Lin, W.C. Wei, J. Am. Ceram. Soc. 89 (2006) 527–533.
[44] Z. Shi, W. Wang, Z. Zhang, Mater. Lett. 62 (2008) 4293–4295.
[45] D.L. Wood, J.S. Tauc, Phys. Rev. B 5 (1972) 3144–3151.
[46] M. Mazzera, M. Zha, D. Calestani, et al., Nanotechnology 18 (2007) 355707.
[47] J.A. Navío, M.C. Hidalgo, G. Colón, S.G. Botta, M.I. Litter, Langmuir 17 (2001) 202–210.
[48] Q. Tang, W. Zhou, W. Zhang, et al., Cryst. Growth Des. 5 (2005) 147–150.
[49] Y. Luo, S. Li, Q. Ren, et al., Cryst. Growth Des. 7 (2007) 87–92.
[50] F.V. Motta, A.T. Figueiredo, V.M. Longo, et al., J. Lumin. 129 (2009) 686–690.
[51] H. Liu, G. Liu, Q. Zhou, et al., Microporous Mesoporous Mater. 142 (2011) 439–443.
[52] Z. Lei, G. Ma, M. Liu, et al., J. Catal. 237 (2006) 322–329.
[53] J. Guo, S. Ouyang, H. Zhou, et al., J. Phys. Chem. C 117 (2013) 17716–17724.
[54] M. Muruganandham, M.E. Sillanpää, R.P. Suri, et al., J. Nanosci. Nanotechnol. 13 (2013) 1639–1648.
[55] T. Yan, J. Long, Y. Chen, et al., C. R. Chim. 11 (2008) 101–106.
[56] Z. Li, T. Dong, Y. Zhang, et al., J. Phys. Chem. C 111 (2007) 4727–4733.
[57] M.A. Herderson, Surf. Sci. Rep. 66 (2011) 185–297.
[58] S.M. Lam, J.C. Sin, A.R. Mohamed, Recent Pat. Chem. Eng. 1 (2008) 209–219.
[59] M.R.D. Bomio, R.L. Tranquilin, F.V. Motta, et al., J. Phys. Chem. C 117 (14) (2013) 21382–21395.